THE JOURNAL OF BIOLOGICAL CHEMISTRY VOL. 288, NO. 13, pp. 9563–9571, March 29, 2013
Published in the U.S.A.

Structural Basis for the Recognition of Tyrosine-based Sorting Signals by the μ3A Subunit of the AP-3 Adaptor Complex*

Received for publication, January 5, 2013, and in revised form, February 1, 2013 Published, JBC Papers in Press, February 12, 2013, DOI 10.1074/jbc.M113.450775

Gonzalo A. Mardones[‡§1], Patricia V. Burgos[‡§], Yimo Lin[§], Daniel P. Kloer[¶2], Javier G. Magadán[§], James H. Hurley[¶3], and Juan S. Bonifacino[§4]

From the [‡]Instituto de Fisiología, Facultad de Medicina, and Centro de Investigación Sur-Austral en Enfermedades del Sistema Nervioso, Universidad Austral de Chile, Valdivia 5110566, Chile, the [§]Cell Biology and Metabolism Program, Eunice Kennedy Shriver, NICHD, National Institutes of Health, Bethesda, Maryland 20892, and the [¶]Laboratory of Molecular Biology, NIDDK, National Institutes of Health, Bethesda, Maryland 20892

Background: Tyrosine-based, Y*XX*Ø-type signals mediate protein sorting through binding to adaptor μ subunits.
Results: X-ray crystallography shows how Y*XX*Ø signals bind to the immunoglobulin-like fold of μ3A.
Conclusion: The binding site for Y*XX*Ø signals on μ3A is similar to that of μ2 but distinct from that of μ4.
Significance: The study explains the basis for the recognition of diverse Y*XX*Ø signals by μ subunits.

Tyrosine-based signals fitting the Y*XX*Ø motif mediate sorting of transmembrane proteins to endosomes, lysosomes, the basolateral plasma membrane of polarized epithelial cells, and the somatodendritic domain of neurons through interactions with the homologous μ1, μ2, μ3, and μ4 subunits of the corresponding AP-1, AP-2, AP-3, and AP-4 complexes. Previous x-ray crystallographic analyses identified distinct binding sites for Y*XX*Ø signals on μ2 and μ4, which were located on opposite faces of the proteins. To elucidate the mode of recognition of Y*XX*Ø signals by other members of the μ family, we solved the crystal structure at 1.85 Å resolution of the C-terminal domain of the μ3 subunit of AP-3 (isoform A) in complex with a peptide encoding a Y*XX*Ø signal (SDYQRL) from the *trans*-Golgi network protein TGN38. The μ3A C-terminal domain consists of an immunoglobulin-like β-sandwich organized into two subdomains, A and B. The Y*XX*Ø signal binds in an extended conformation to a site on μ3A subdomain A, at a location similar to the Y*XX*Ø-binding site on μ2 but not μ4. The binding sites on μ3A and μ2 exhibit similarities and differences that account for the ability of both proteins to bind distinct sets of Y*XX*Ø signals. Biochemical analyses confirm the identification of the μ3A site and show that this protein binds Y*XX*Ø signals with 14–19 μM affinity. The surface electrostatic potential of μ3A is less basic than that of μ2, in part explaining the association of AP-3 with intracellular membranes having less acidic phosphoinositides.

Sorting of transmembrane proteins to different compartments of the endomembrane system is most often mediated by recognition of signals in the cytosolic domains of the proteins by adaptor molecules that are components of protein coats (1). Recognition leads to selective incorporation of the transmembrane proteins into coated vesicles that serve as vehicles for intercompartmental transport. Studies over the past three decades have identified a variety of sorting signals and adaptors that participate in different transport steps. Many signals are linear arrays of amino acids that fit one of several canonical motifs (2). Among them, tyrosine-based signals conforming to the Y*XX*Ø motif (where *X* is any amino acid and Ø is an amino acid with a bulky hydrophobic side chain) (3) have prominent roles in endocytosis (4), as well as sorting to lysosomes (5), the basolateral plasma membrane of polarized epithelial cells (6), and the somatodendritic domain of neurons (7). Y*XX*Ø signals are recognized by the homologous μ1, μ2, μ3, and μ4 subunits of the heterotetrameric adaptor protein (AP)[5] complexes AP-1 (γ-β1-μ1-σ1), AP-2 (α-β2-μ2-σ2), AP-3 (δ-β3-μ3-σ3), and AP-4 (ε-β4-μ4-σ4), respectively (subunit composition in parenthesis) (8–12). The μ1 and μ3 subunits occur as two isoforms (denoted A and B) that are encoded by different genes. The amino acid sequence identity among μ subunits from different AP complexes is 25–38%, whereas that of μ1 and μ3 isoforms is 79–84%. All of the μ subunits have a conserved organization consisting of an N-terminal domain that mediates assembly into the corresponding AP complex and a C-terminal domain that binds subsets of Y*XX*Ø signals (13). Two other proteins, the μ5 subunit of the AP-5 complex (14) and the δ subunit of the COPI complex (15), are homologous to the AP-μ subunits over their entire sequence, but to date they have not been shown to recognize any signals. Finally, several monomeric proteins, including the human proteins Stonin 1 and Stonin 2 (16, 17), and FCHO1, FCHO2, and SGIP1 (18), have a

* This work was supported by Grant 1100896 from Fondo Nacional de Desarrollo Científico y Tecnológico of Chile (to G. A. M.), and the Intramural Programs of NICHD (to J. S. B.) and NIDDK (to J. H. H.), National Institutes of Health. Use of the Advanced Photon Source was supported by the U. S. Department of Energy, Basic Energy Sciences, Office of Science under Contract W-31-109-Eng-38.

The atomic coordinates and structure factors (code 4IKN) have been deposited in the Protein Data Bank (http://wwpdb.org/).

[1] To whom correspondence may be addressed. Tel: 56-63-293129; Fax: 56-63-221513; E-mail: gonzalo.mardones@uach.cl.

[2] Present address: Syngenta Jealott's Research Centre, Bracknell RG42 6EY, United Kingdom.

[3] To whom correspondence may be addressed. Tel.: 301-402-4703; Fax: 301-480-2282; E-mail: hurley@helix.nih.gov.

[4] To whom correspondence may be addressed. Tel.: 301-496-6368; Fax: 301-402-0078; E-mail: juan@helix.nih.gov.

[5] The abbreviations used are: AP, adaptor protein; ITC, isothermal titration calorimetry; MHC-I, MHC class I; Y2H, yeast two-hybrid; TGN, *trans*-Golgi network; PDB, Protein Data Bank.

domain that is homologous to the C-terminal domain of the μ subunits. These proteins also function as cargo adaptors, although likely through recognition of folded structures rather than linear motifs, as shown for Stonin 2 (16, 17) and FCHO1 (19).

X-ray crystallographic analyses have provided insights into the mechanisms of signal recognition by μ1A, μ2, and μ4 (20–22). The C-terminal domain of these proteins consists of an elongated immunoglobulin-like β-sandwich fold with 16 β-strands organized into two subdomains (A and B). In μ2, Y*XX*Ø signals bind to a site on strands β1 and β16 in subdomain A, with the Y and Ø residues fitting into two hydrophobic pockets (20). The structure of μ1A was solved as part of a ternary complex with the cytosolic tail of an MHC class I (MHC-I) molecule and the Nef protein of HIV-1. The MHC-I tail has a Tyr residue that fits into a pocket similar to that in μ2 but lacks an Ø residue that could bind to the other pocket (22). Instead, both the MHC-I tail and Nef establish additional interactions with other parts of μ1A (22). Of the μ subunits that have been characterized to date, μ4 exhibits the most distinct specificity of Y*XX*Ø signal recognition. Although μ4 weakly binds some generic Y*XX*Ø signals (10, 11, 12), it displays a strong preference for a subset of Y*XX*Ø signals fitting the Y*X*(FYL)(FL)E motif, which occur in the cytosolic tails of members of the amyloid precursor protein family (21). Surprisingly, the latter signals bind to a distinct site located on strands β4, β5, and β6 in subdomain A, which also has hydrophobic pockets for the Tyr and (FL) residues (21). The crystal structure of μ4 predicts the presence of an additional site similar to that on μ2 (21). Mutations in this site abolish the weak binding of a canonical Y*XX*Ø signal (YEQF) from the lysosomal membrane protein Lamp-2 (12), suggesting that this site also functions in signal recognition. Thus, μ4 has two binding sites for Y*XX*Ø signals on opposite faces of subdomain A. This raises the possibility that other μ subunits have more than one signal-binding site as well.

The μ3A and μ3B subunit isoforms also bind Y*XX*Ø signals (9, 23, 24), but the structural basis for this recognition remains to be elucidated. In light of the diversity of Y*XX*Ø-binding modes, outstanding questions concern the location and characteristics of the Y*XX*Ø-binding site on μ3A and μ3B. To address these questions, we solved the crystal structure of the C-terminal domain of μ3A in complex with a Y*XX*Ø-containing peptide from the *trans*-Golgi network (TGN)-localized protein TGN38 at 1.85 Å resolution. We found that the C-terminal domain of μ3A possesses an immunoglobulin-like β-sandwich fold made up of 16 strands, similar to the C-terminal domains of μ1A (22) μ2 (20), and μ4 (21). The TGN38 peptide binds to μ3A at a site equivalent to that on μ2, albeit with fewer stabilizing contacts. Yeast two-hybrid (Y2H) analyses validated the identity of this binding site and, consistent with the crystallographic data, isothermal titration calorimetry (ITC) showed that μ3A has lower affinity for Y*XX*Ø signals relative to μ2. Analysis of the surface of μ3A revealed a less basic electrostatic potential compared with that of μ2, providing a likely explanation for the preference of AP-3 for binding to endosomes rather than the plasma membrane (24–26).

EXPERIMENTAL PROCEDURES

Recombinant DNAs, Site-directed Mutagenesis, and Y2H Assays—To generate a His_6-fusion construct with the C-terminal domain of μ3A, the sequence encoding residues 165–418 of rat μ3A was amplified by PCR and cloned in-frame into the EcoRI and SalI sites of pHis-Parallel-1 (27). TGN38, CD63, and Lamp-1 constructs for Y2H assays were described previously (12). Single amino acid substitutions were introduced using the QuikChange mutagenesis kit (Stratagene, La Jolla, CA). The nucleotide sequences of all recombinant constructs were confirmed by dideoxy sequencing. Y2H assays were performed as described previously (21).

Expression and Purification of μ3A C-terminal Domain Constructs—Recombinant μ3A C-terminal domain (μ3A-C) constructs tagged with an N-terminal His_6 tag followed by a Tobacco edge virus protease cleavage site were expressed in *Escherichia coli* B834(DE3)pLysS (Novagen, Madison, WI) after induction with 0.5 mM isopropyl 1-thio-β-D-galactopyranoside at 25 °C for 16 h. Pellets were resuspended in 50 mM Tris-HCl (pH 8.0), 0.5 M NaCl, 5 mM β-mercaptoethanol and protease inhibitors (Sigma-Aldrich), and lysed by sonication. The clarified supernatant was purified on nickel-nitrilotriacetic acid resin (Qiagen, Valencia, CA) and eluted with 300 mM imidazole. N-terminal, His_6-tagged Tobacco edge virus protease was used to cleave the His_6 moiety from μ3A-C. The His_6 moiety and His_6-tagged Tobacco edge virus were removed by an additional passage through nickel-nitrilotriacetic acid resin, and μ3A-C was further purified on a Superdex 200 column (GE Healthcare) equilibrated with buffer containing 25 mM Tris-HCl (pH 8.0), 150 mM NaCl, 5% glycerol, and 2.5 mM β-mercaptoethanol.

Crystallization, Data Collection, and Structure Determination—Unless otherwise stated, solutions and crystallization reagents were from Hampton Research (Aliso Viejo, CA). Crystals of the μ3A C-terminal domain in complex with the TGN38 peptide SDYQRL (New England Peptide, Gardner, MA) were grown by the hanging drop method at 21 °C. The reservoir solution contained 0.1 M sodium acetate (pH 5.0) and 1.75 M sodium formate. Drops contained 1 μl of reservoir solution and 1 μl of 5 mg/ml protein-peptide complex. Prior to crystallization, the protein was incubated at room temperature for 1 h with 2.5 mM peptide. Under these conditions, crystals appeared after 48–60 h. Crystals were cryoprotected in the reservoir solution supplemented with 30% glycerol and then flash-cooled in liquid nitrogen. Crystals belonged to space group *C*2 and diffracted to 1.85 Å resolution. The structure was determined by molecular replacement using as search model rat μ2 C-terminal domain (PDB code 1BXX) (20). A native data set was collected from a single crystal using a MAR CCD detector at the SER-CAT beamline 22-ID at Advanced Photon Source, Argonne National Laboratory. Diffraction images were processed and scaled with the program HKL2000 (28). Data collection statistics are shown in Table 1. Iterative manual model building and initial refinement were done using COOT (29) and REFMAC. The final model has a single chain of 248 residues with 136 water molecules, and five residues (DYQRL) from the TGN38 cytosolic tail peptide. Molecular model figures were generated with PyMOL

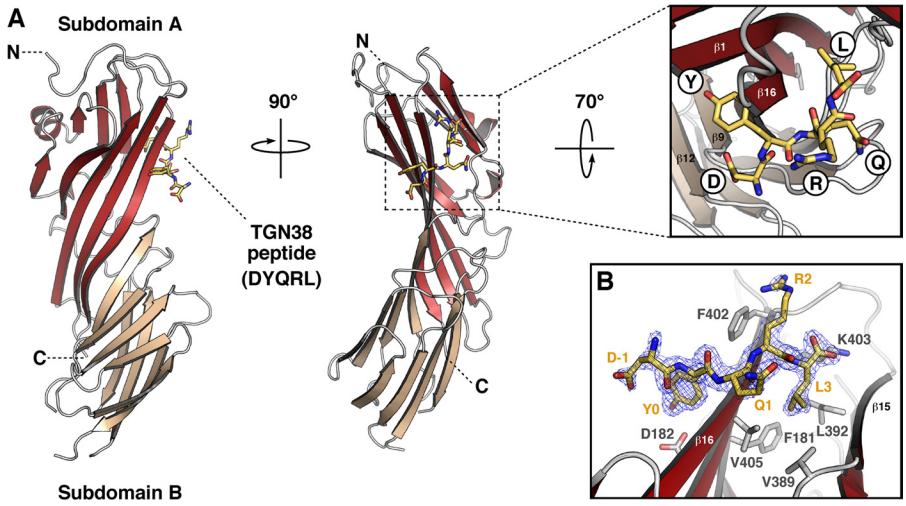

FIGURE 1. **Crystal structure of the μ3A C-terminal domain in complex with a Y*XX*Ø-encoding peptide from TGN38.** *A*, ribbon representation of rat μ3A C-terminal domain with subdomain A in *brick red*, subdomain B in *salmon*, and the TGN38 peptide (DYQRL; stick model) in *yellow*. The *inset* shows the location of the peptide side chains on the binding site. The position of the N (*N*) and C (*C*) termini are indicated. *B*, stick representation of the bound peptide DYQRL (shown with carbon atoms colored *yellow*) superimposed on a $2F_o - F_c$ omit electron density map contoured at 1.5σ, and μ3A binding site amino acid residues are highlighted in stick representation (shown with carbon atoms colored *gray*).

software. Crystallographic coordinates and structure factors have been deposited in the Protein Data Bank under 4IKN.

Isothermal Titration Calorimetry—Recombinant μ3A-C constructs were dialyzed overnight at 4 °C against excess ITC buffer (50 mM Tris-HCl, pH 7.4, 150 mM NaCl). TGN38 and CD63 peptides (SDYQRL, SDAQRL, SGYEVM, and SGAEVM; New England Peptide) were also prepared in ITC buffer. All ITC experiments were carried out at 28 °C using an iTC_{200} instrument (MicroCal LLC, Northampton, MA). Typically, the chamber contained 0.2 ml of 100–375 μM μ3A-C constructs, and the peptides (1–3.75 mM) were added in 18 injections of 2.45-μl each. Titration curves were analyzed using Origin software (MicroCal). The binding constant was calculated by fitting the curves corresponding to μ3A-C to a one-site model.

RESULTS AND DISCUSSION

We solved the crystal structure of the C-terminal domain of rat μ3A (residues 165–418) in complex with a SDYQRL peptide derived from the cytosolic tail of rat TGN38 at 1.85 Å resolution (Fig. 1 and Table 1). The SDYQRL peptide encodes a Y*XX*Ø signal in which the tyrosine residue is referred to as Y0 (position 0 corresponds to the most critical residue of the motif) and the leucine residue at the Ø position is denoted as L3 (position +3 from Tyr-0). Similar to μ1A (22, 30), μ2 (20), and μ4 (21), the μ3A C-terminal domain has an immunoglobulin-like β-sandwich fold consisting of 16 strands organized into two subdomains, A and B (Fig. 1*A* and Figs. 2 and 3). The overall root mean square deviation for superimposable Cα coordinates for the C-terminal domain of μ3A and the C-terminal domain of the other μ subunits is 1.50 Å for μ1A, 1.70 Å for μ2, and 3.65 Å for μ4 (Fig. 2).

Only the DYQRL segment from the peptide is visible in the density map (Fig. 1*B*). This segment binds in an extended conformation to parallel strands β1 and β16 of μ3A subdomain A (Fig. 1, *A* and *B*), similarly to the binding of the TGN38 peptide to μ2 (Figs. 2*B* and 4) (20). Two hydrophobic pockets accommodate the Y0 and L3 residues of the signal on either side of strand β16 (Figs. 1 and 4). The signal-binding site on μ3A (Figs. 1, 2, and 4*C*) is at a location similar to that on μ1A (22) and μ2 (20) (Figs. 2, *A* and *B*, and 4*A*). It differs, however, from the binding site for Y*X*(FYL)(FL)E signals on μ4, which is on the opposite face of the protein (Fig. 2*C*) (21). The area of the interface involving the Y*XX*Ø signal from TGN38 is 416 $Å^2$ on μ3A and 434 $Å^2$ on μ2, comparable with that of the Y*X*(FYL)(FL)E signal bound to μ4, which is 431 $Å^2$, as calculated by the PISA server (31).

The μ3A-Y*XX*Ø signal interface has substantial polar character, with four direct hydrogen bonds (distance ≤ 3.1 Å) between peptide and protein (Fig. 4*D*); this polarity is lower than that of the μ2-Y*XX*Ø signal interface, which has seven direct hydrogen bonds (Fig. 4*B*). The phenolic hydroxyl group of Y0 forms the shortest side chain to side chain hydrogen bond with the carboxylate of Asp-182 in μ3A (Fig. 4*D*). The critical role of this interaction was demonstrated by Y2H analyses. Substitution of alanine for Y0 in the Y*XX*Ø motif from the cytosolic tails of TGN38 or the lysosomal membrane proteins CD63 (YEVM) or Lamp-1 (YQTI) completely abolished binding to

TABLE 1
Statistics of crystallographic data collection and refinement
Values in parentheses refer to the highest resolution shell. r.m.s., root mean square.

Data collection	
Space group	*C*2
Unit cell parameters	$a = 114.5$, $b = 44.3$, $c = 86.0$ Å; $\beta = 127.8°$
Wavelength (Å)	1.0000
Resolution (Å)	1.85 (1.92–1.85)
No. of reflections	124,475
No. of unique reflections	28591
$I/\sigma(I)$	19.9 (3.2)
Data completeness (%)	97.6 (85.7)
Redundancy	4.4 (3.3)
R_{sym} (%)[a]	6.4 (32.3)
Structure refinement	
R_{factor} (%)	19.1
R_{free} (%)[b]	23.8
r.m.s. bond lengths (Å)	0.026
r.m.s. bond angles	2.104°

[a] $R_{sym} = \Sigma_{hkl}|I_{hkl} - \langle I_{hkl}\rangle|/\Sigma_{hkl}I_{hkl}$.
[b] R_{free} = free R_{factor} based on random 5% of all data.

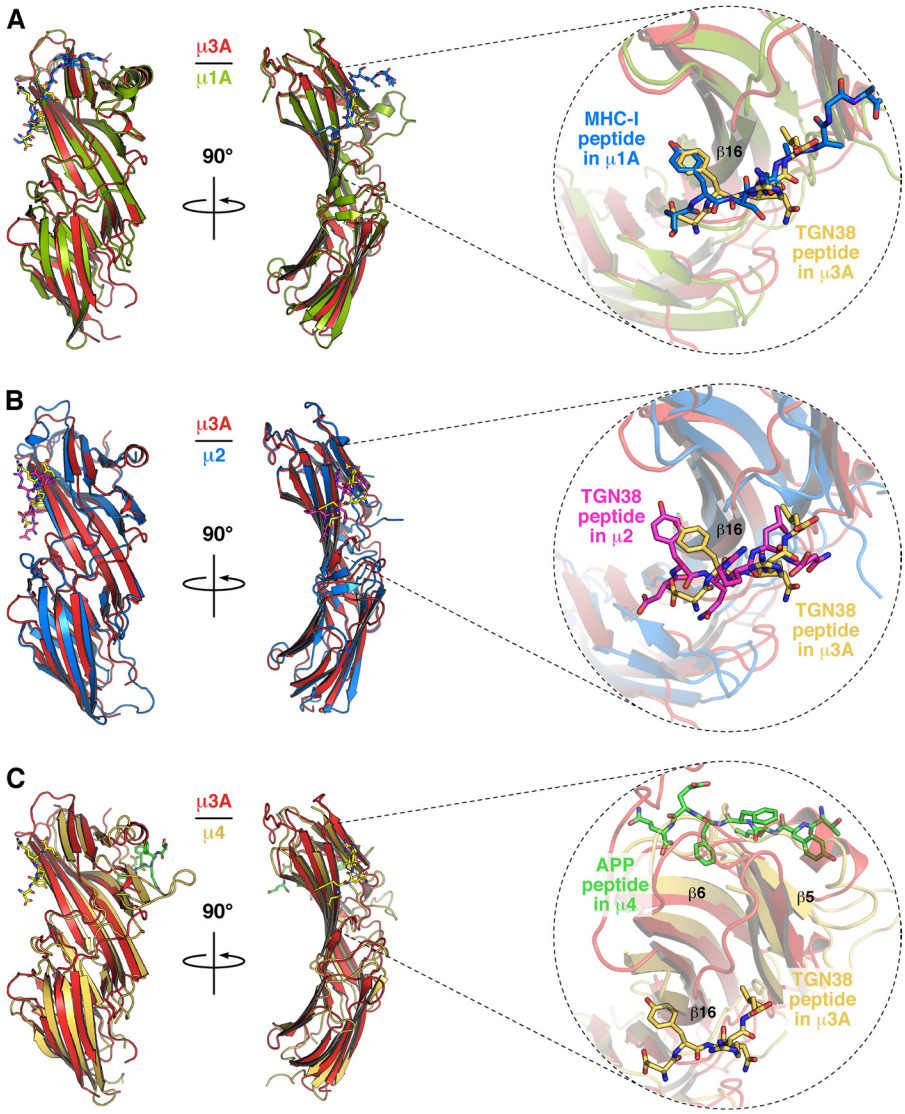

FIGURE 2. **Comparison of the crystal structure of μ subunits.** *A*, superposition of rat μ3A (*red*) and mouse μ1A (*green*; PDB code 4EN2) (22). *B*, superposition of μ3A (*red*) and rat μ2 (*blue*; PDB code 1BXX) (20); and *C*, superposition of μ3A (*red*) and human μ4 (*orange*; PDB code 3L81 (21) shown in ribbon representation. The bound peptides SYSQAAGSDSAQ on μ1A (shown with carbon atoms colored *blue*; oxygen colored *red*; nitrogen colored *blue*), DYQRLN on μ2 (carbon atoms colored *magenta*), DYQRL on μ3A (carbon atoms colored *yellow*), and TYKFFEQ on μ4 (carbon atoms colored *green*) are shown in stick representation.

μ3A (Fig. 5*A*). Reciprocally, substitution of alanine or serine for Asp-182 in μ3A precluded binding to the TGN38, CD63 and Lamp-1 signals (Fig. 5*B*). These determinants of interaction were confirmed *in vitro* by ITC using purified components. We found that a synthetic TGN38 SDYQRL peptide, but not a substituted SDAQRL variant, bound to a single site on recombinant μ3A C-terminal domain with K_d of 14.0 ± 2.8 μM (Fig. 6*A*). Similarly, a synthetic CD63 SGYEVM peptide, but not a substituted SGAEVM variant, bound to a single site with K_d of 18.7 ± 1.6 μM (Fig. 6*B*). Single substitution of serine for Asp-182 rendered the interaction with both peptides undetectable (Fig. 6, *A* and *B*).

In addition to hydrogen bonds, there are hydrophobic interactions between Tyr-0 in the peptide and Tyr-180 and Phe-402 of μ3A, as well as stacking on the side chain of Lys-406 of μ3A (Fig. 4, *C* and *D*). Y2H analyses showed that the interaction of Y*XXØ* signals from TGN38, CD63, or Lamp-1 with μ3A was completely abrogated by substitution of alanine for Tyr-180 or serine for Phe-402 (Fig. 5*B*). Substitution of alanine for Lys-406 resulted in varied effects, with interaction with TGN38 being seemingly unaffected, Lamp-1 completely abolished, and CD63 partially diminished (Fig. 5*B*). The differential effects of the Lys-406 mutation inversely correlate with the overall binding affinity of the signals (TGN38 > CD63 > Lamp-1) (Figs. 5 and 6), a fact that can be explained by the loss of the hydrophobic stacking interaction on Y0 having a greater effect on the weaker signals.

Unlike μ2, in which the hydroxyl group of Y0 participates in a network of hydrogen bonds with Asp-176, Lys-203, and Arg-423 (Fig. 4, *A* and *B*) (20), in μ3A, the hydroxyl group of Y0 forms a hydrogen bond only with Asp-182 (Fig. 4, *C* and *D*). In place of μ2 Lys-203, μ3A contains Cys-209, which is too far to contribute to the binding of Y0 (Figs. 3 and 4*C*). Consistent with this observation, Y2H analysis showed that substitution of alanine for Cys-209 did not affect the interaction of μ3A with

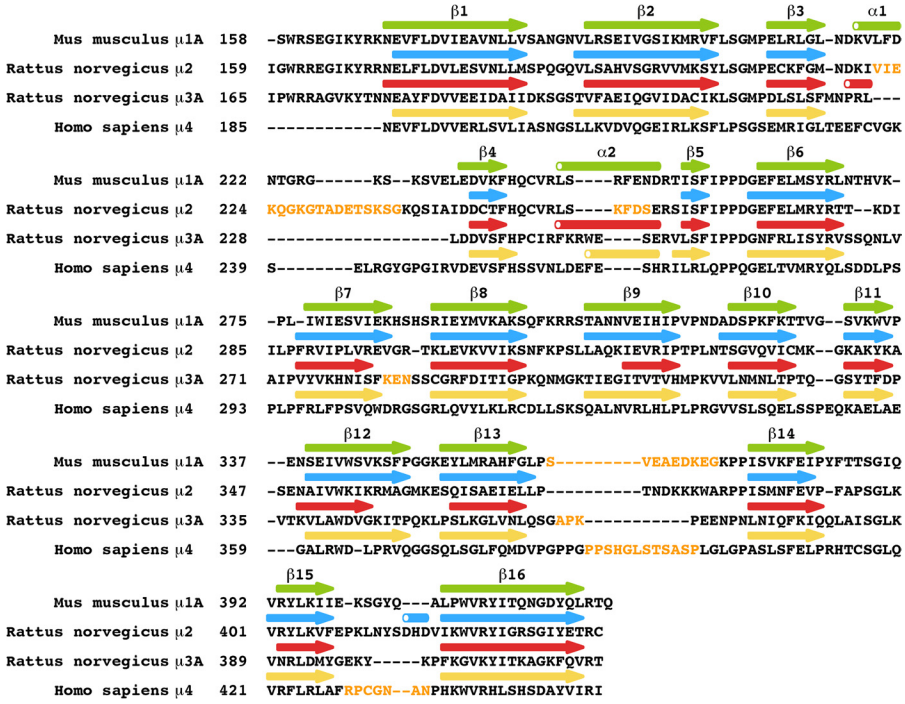

FIGURE 3. **Sequence alignment of the C-terminal domains of the μ subunits.** Disordered loops are in *yellow letters*. *Arrows* and *cylinders* represent β-strands and α-helices, respectively.

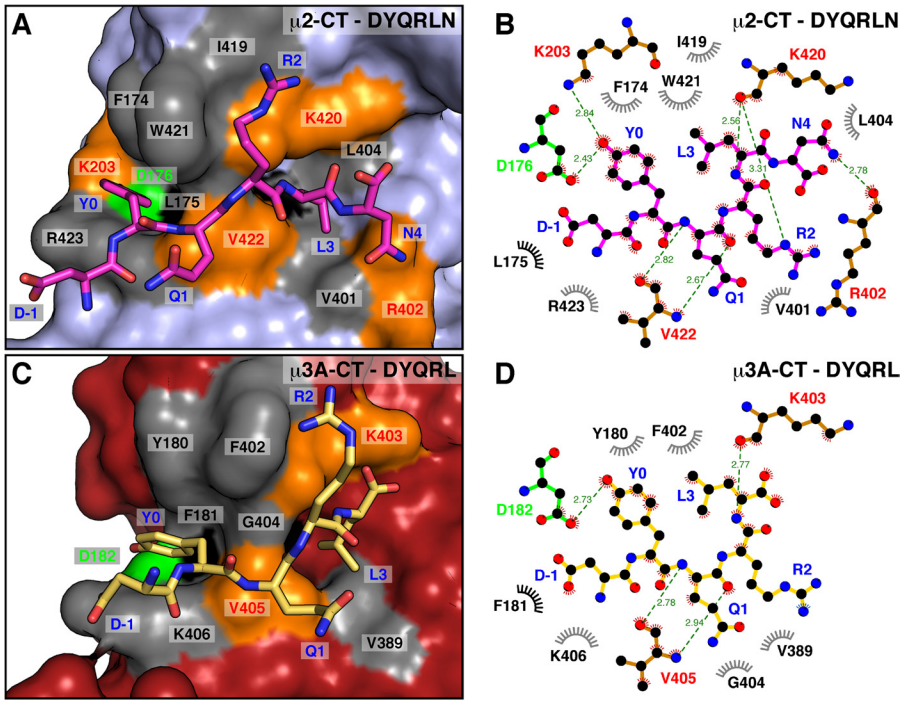

FIGURE 4. **Comparison of the binding site for the TGN38 *YXXØ* motif in μ2 and μ3A.** *A* and *C*, surface complementarity between TGN38 peptides and μ2 (*A*) and μ3A (*C*). Surface colors for residues in contact with the TGN38 peptide are *gray* for hydrophobic interactions, except for Leu-175 in μ2 and Phe-181 in μ3A that are colored *black*. Residues forming hydrogen bonds are colored *orange*, except for Asp-176 in μ2 and Asp-182 in μ3A, which are colored *green*. The bound peptides DYQRLN on μ2 (shown with carbon atoms colored *magenta*; oxygen is colored *red*; nitrogen is colored *blue*; PDB code 1BXX) and DYQRL on μ3A (carbon atoms colored *yellow*) are shown in stick representation. *B* and *D*, two-dimensional, schematic representation of the interactions shown in *A* and *C* using LIGPLOT (48).

YXXØ signals from TGN38 or CD63 (Fig. 5*B*). Interaction with Lamp-1, however, was reduced (Fig. 5*B*).

The binding pocket for the peptide L3 is lined by the aliphatic side chains of Phe-181, Val-389, and Leu-392 in μ3A (Fig. 4, *C* and *D*). The size of this pocket accommodates L3 in the same way as the pocket formed by Leu-175, Val-401, and Leu-404 in μ2 (Fig. 4, *A* and *B*) (20). Peptide library screening has revealed a preference for an arginine residue at position Y+2 (Arg-2) (9). In μ3A, R2 forms mainly hydrophobic interactions with Phe-402. In contrast, in μ2 R2 is stabilized by hydrophobic interac-

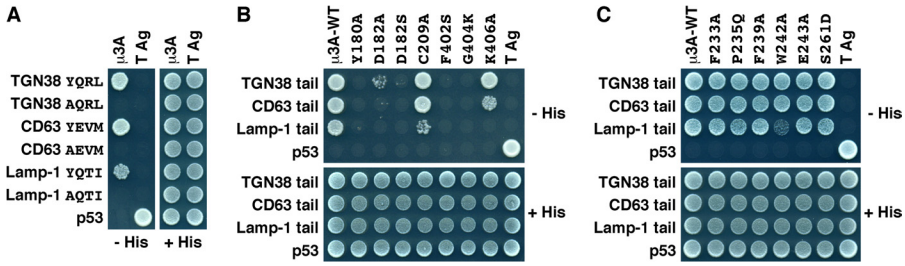

FIGURE 5. **Y2H analysis of the interaction of μ3A with cytosolic tails containing a Y*XX*Ø motif.** *A–C*, yeast were co-transformed with plasmids encoding Gal4bd fused to the wild-type or Tyr-to-Ala mutant of the cytosolic tails of TGN38, CD63, or Lamp-1 constructs indicated on the *left*, and Gal4ad fused to wild-type or mutant μ3A constructs indicated on *top* of each *panel*. *B*, Y2H analysis of μ3A with mutations on the Y*XX*Ø-binding site. *C*, Y2H analysis of μ3A with mutations on a putative YX(FYL)(FL)E-binding site. Mouse p53 fused to Gal4bd and SV40 large T antigen (*T Ag*) fused to Gal4ad were used as controls. Co-transformed cells were spotted onto His-deficient (−His) or His-containing (+His) plates and incubated at 30 °C. Growth is indicative of interactions.

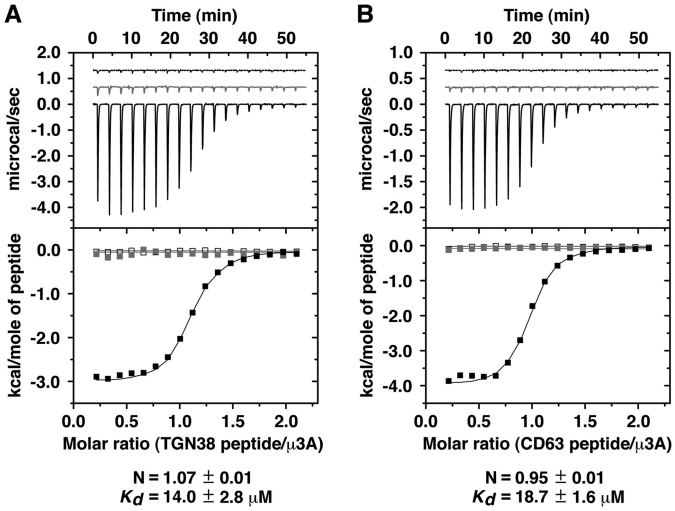

FIGURE 6. **ITC analysis of the interaction of μ3A with peptides containing a Y*XX*Ø motif.** *A*, ITC of the TGN38 SDYQRL peptide (*black line* and *solid squares*) or SDAQRL peptide (*gray line* and *gray squares*) with μ3A, and of SDYQRL peptide with μ3A D182A (*dashed line* and *open squares*). *B*, ITC of the CD63 SGYEVM peptide (*black line* and *solid squares*) or SGAEVM peptide (*gray line* and *gray squares*) with μ3A, and of SGYEVM peptide with μ3A D182A (*dashed line* and *open squares*). The stoichiometry (*N*) and K_d for the μ3A-SDYQRL and for the μ3A-SGYEVM interactions are expressed as the mean ± S.E. ($n = 3$).

tions with Ile-419 and Trp-421, but also by hydrogen bonding between its Nϵ and the carbonyl group of Lys-420 (Fig. 4, *A* and *B*) (20). It has been suggested that replacement of Trp-421 in μ2 by Gly-404 in μ3A would remove the specificity for arginine at the Y+2 position (20). However, both Gly-404 and Phe-402 (Fig. 4, *C* and *D*) contribute to binding, as their substitution by lysine and alanine, respectively, abrogates binding to the Y*XX*Ø signals from TGN38, CD63, and Lamp-1 in Y2H assays (Fig. 5*B*).

Because the Y*X*(FYL)(FL)E-type signal from amyloid precursor protein (YKFFE) binds to a different site on μ4 (21), it was of interest to test whether residues on the equivalent site on μ3A played any role in the recognition of Y*XX*Ø signals from TGN38, CD63, and Lamp-1. Y2H assays showed that single substitution of Phe-255 to alanine or Arg-283 to aspartate drastically reduced binding of the amyloid precursor protein tail to μ4 (21). In contrast, single substitution of the corresponding Phe-233 to alanine or Ser-261 to aspartate in μ3A did not affect binding to Y*XX*Ø signals from TGN38, CD63, and Lamp-1 (Fig. 5*C*). Likewise, single mutation of other residues predicted to be in this binding site, such as Pro-235 to glutamine, Phe-239 to alanine, Trp-242 to alanine, or Glu-243 to alanine, produced essentially no effect on the binding of μ3A to the Y*XX*Ø signals (Fig. 5*C*). This corroborates and extends the structural finding that the Y*XX*Ø signals bind to μ3A exclusively through the conserved, canonical binding site revealed by the crystal structure.

AP complexes are organized as a "core" with two "hinge -ear" projections. Structural analyses have shown that the AP-2 core occurs in two conformations: a locked conformation in which the binding sites for Y*XX*Ø signals and for dileucine-based sorting signals fitting the (DE)*XXX*L(LI) motif are occluded by the β2 subunit of the complex and an open conformation in which both sites are accessible for binding (Fig. 7, *A* and *E*) (32–34). The structure of the AP-3 core has not yet been solved but, based on structural homology, the Y*XX*Ø-binding site in μ3A would likewise be expected to be accessible in the open core conformation (Fig. 7, *C* and *G*).

The basic electrostatic potential of μ2 near the binding site for the Y*XX*Ø motif in the open conformation of the AP-2 core has been postulated to be important for interaction with the negatively charged head groups of phosphatidylinositol 4,5-bisphosphate at the plasma membrane (Fig. 7, *A* and *E*) (34, 35). The same region has a considerably lower positive electrostatic potential in μ3A (Fig. 7*G*), as well as in μ1A and μ4 (Fig. 7, *F* and *H*). Unlike AP-2, which binds phosphatidylinositol 4,5-bisphosphate, AP-1 and AP-3 preferentially bind to the less negatively charged phosphatidylinositol 4-phosphate and phosphatidylinositol 3-phosphate, respectively (36, 37). In particular, phosphatidylinositol 4,5-bisphosphate binding residues Lys-341, Lys-343, Lys-345, and Lys-354 in μ2 are replaced by Ser-329, Thr-331, Asp-333, and Asp-342 in μ3A (Fig. 7, *I* and *J*). These differences might contribute to the preferential binding of AP-1 and AP-3 to intracellular membranes enriched in less acidic phospholipids.

The ability of μ3A to recognize Y*XX*Ø signals explains the requirement of AP-3 for efficient sorting of a subset of lysosomal membrane proteins such as CD63, Lamp-1, and Lamp-2 from endosomes to lysosomes in various cell types (26, 38, 39). This activity may also contribute to the sorting of Y*XX*Ø-containing proteins to lysosome-related organelles such as pigment granules/melanosomes and platelet-dense bodies, a process in which AP-3 is critically involved (38, 40–42). In this regard, it is noteworthy that the affinity of Y*XX*Ø-signal binding to μ3A (Fig. 6) is one order of magnitude lower than that of μ2 (43),

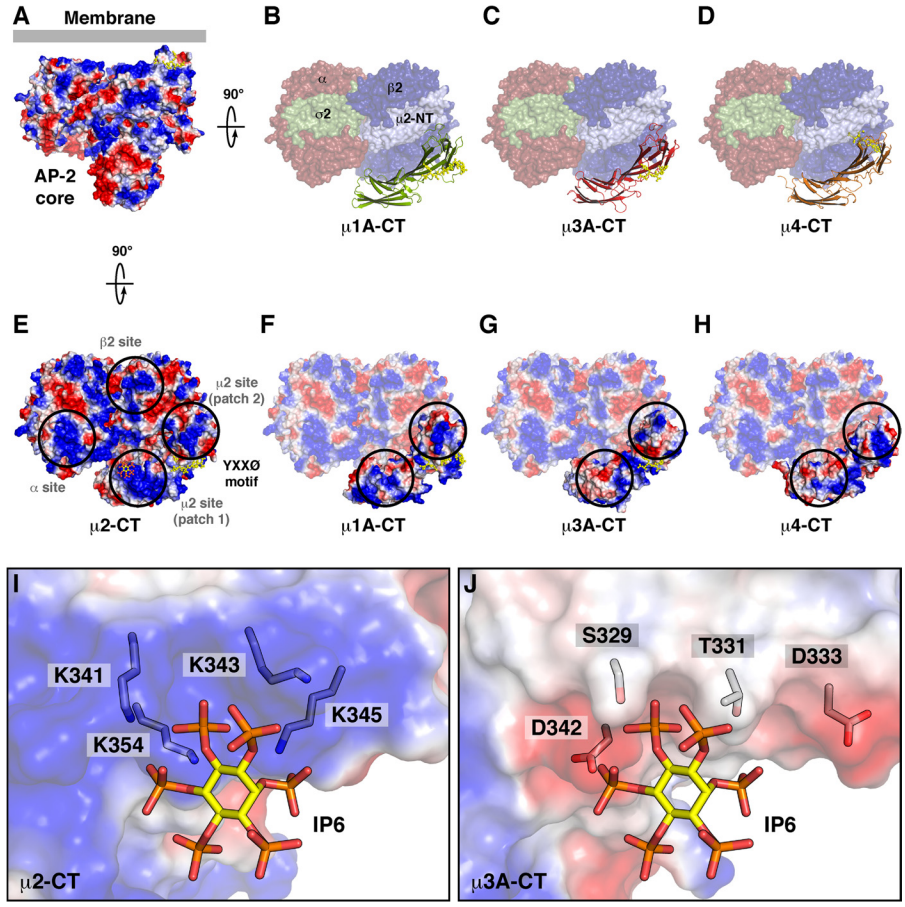

FIGURE 7. **Comparison of the surface electrostatic potential of μ subunits.** *A* and *E*, two views of AP-2 complex core in the open conformation on the membrane and colored by electrostatic potential (34), with inositol 6-phosphate (*IP6*) in stick representation bound to a μ2 site (patch 1; *E*). *B–D*, surface representation of the orthogonal view of the structure shown in *A* colored by subunit (α, *red*; β2, *blue*; N-terminal domain of μ2, *pale blue*; σ2, *green*) and ribbon representation of the C-terminal domain of the indicated μ subunits superposed on the site equivalent to that of μ2 C-terminal domain. *F–H*, electrostatic potential of the C-terminal domain of the indicated μ subunits superposed as in *B–D*. Peptides with a YXXØ or a related motif are shown in stick representation colored *yellow*. *Blue* and *red* correspond to positive and negative potentials, respectively, with saturating color at ±5 kT/e. *Black circles* indicate positive patches on AP-2 for interaction with phospholipids (*E*) and equivalent patches on other μ subunits (*F–H*). *I* and *J*, comparison of the binding site for inositol 6-phosphate on the surface of μ2 (*I*), and the respective surface of μ3A (*J*), colored by electrostatic potential, showing inositol 6-phosphate and side chains in stick representation (carbon atoms in IP6 colored *yellow*; carbon atoms in side chains colored *gray*; oxygen colored *red*; nitrogen colored *blue*; phosphorus colored *orange*).

consistent with the smaller number of interactions that stabilize the binding of YXXØ signals to μ3A (Fig. 4). This difference is in line with results from previous combinatorial Y2H screens showing that μ2 exhibits the strongest binding and broadest specificity for YXXØ signals among all μ family members (9, 12). We believe that this explains why most YXXØ signals mediate AP-2-dependent endocytosis, whereas only a subset function in AP-3-dependent intracellular sorting events (2). The lower affinity of μ3A relative to μ2 might also explain the observation that changing the spacing of the YXXØ signal relative to the transmembrane domain of Lamp-1, a manipulation that affects optimal presentation of the signal, decreases transport from endosomes to lysosomes without affecting the rate of endocytosis (44).

The μ3A structure presented here corresponds to the first portion of the AP-3 complex and only the second μ subunit (after μ2) in complex with a canonical YXXØ signal to be solved by x-ray crystallography. Our findings allow us to demonstrate the conservation of the canonical YXXØ binding site and thus the generality of the signal-recognition mode first shown for μ2 (20). Biochemical and structural analyses indicate that μ1 (A and B isoforms) (7, 22, 45) and μ4 (12) are likely to have a similar binding site (21, 22, 30, 45–47), but this remains to be definitively established by x-ray crystallographic studies of μ1 and μ4 in complex with canonical YXXØ signals. It also remains to be determined whether μ1, μ2, and μ3 have a second site similar to that binding YX(FYL)(FL)E signals in μ4 (21).

Acknowledgments—We thank X. Zhu and N. Tsai for excellent technical assistance and the staff of the SER-CAT 22-ID beamline at the Advanced Photon Source, Argonne National Laboratory for assistance with x-ray data collection.

REFERENCES

1. Kirchhausen, T., Bonifacino, J. S., and Riezman, H. (1997) Linking cargo to vesicle formation: receptor tail interactions with coat proteins. *Curr. Opin. Cell Biol.* **9,** 488–495
2. Bonifacino, J. S., and Traub, L. M. (2003) Signals for sorting of transmembrane proteins to endosomes and lysosomes. *Annu. Rev. Biochem.* **72,** 395–447

3. Canfield, W. M., Johnson, K. F., Ye, R. D., Gregory, W., and Kornfeld, S. (1991) Localization of the signal for rapid internalization of the bovine cation-independent mannose 6-phosphate/insulin-like growth factor-II receptor to amino acids 24–29 of the cytoplasmic tail. *J. Biol. Chem.* **266,** 5682–5688
4. Collawn, J. F., Stangel, M., Kuhn, L. A., Esekogwu, V., Jing, S. Q., Trowbridge, I. S., and Tainer, J. A. (1990) Transferrin receptor internalization sequence YXRF implicates a tight turn as the structural recognition motif for endocytosis. *Cell* **63,** 1061–1072
5. Guarnieri, F. G., Arterburn, L. M., Penno, M. B., Cha, Y., and August, J. T. (1993) The motif Tyr-*X*-*X*-hydrophobic residue mediates lysosomal membrane targeting of lysosome-associated membrane protein 1. *J. Biol. Chem.* **268,** 1941–1946
6. Höning, S., and Hunziker, W. (1995) Cytoplasmic determinants involved in direct lysosomal sorting, endocytosis, and basolateral targeting of rat lgp120 (lamp-I) in MDCK cells. *J. Cell Biol.* **128,** 321–332
7. Farías, G. G., Cuitino, L., Guo, X., Ren, X., Jarnik, M., Mattera, R., and Bonifacino, J. S. (2012) Signal-mediated, AP-1/clathrin-dependent sorting of transmembrane receptors to the somatodendritic domain of hippocampal neurons. *Neuron* **75,** 810–823
8. Ohno, H., Stewart, J., Fournier, M. C., Bosshart, H., Rhee, I., Miyatake, S., Saito, T., Gallusser, A., Kirchhausen, T., and Bonifacino, J. S. (1995) Interaction of tyrosine-based sorting signals with clathrin-associated proteins. *Science* **269,** 1872–1875
9. Ohno, H., Aguilar, R. C., Yeh, D., Taura, D., Saito, T., and Bonifacino, J. S. (1998) The medium subunits of adaptor complexes recognize distinct but overlapping sets of tyrosine-based sorting signals. *J. Biol. Chem.* **273,** 25915–25921
10. Stephens, D. J., and Banting, G. (1998) Specificity of interaction between adaptor-complex medium chains and the tyrosine-based sorting motifs of TGN38 and lgp120. *Biochem. J.* **335,** 567–572
11. Hirst, J., Bright, N. A., Rous, B., and Robinson, M. S. (1999) Characterization of a fourth adaptor-related protein complex. *Mol. Biol. Cell* **10,** 2787–2802
12. Aguilar, R. C., Boehm, M., Gorshkova, I., Crouch, R. J., Tomita, K., Saito, T., Ohno, H., and Bonifacino, J. S. (2001) Signal-binding specificity of the mu4 subunit of the adaptor protein complex AP-4. *J. Biol. Chem.* **276,** 13145–13152
13. Aguilar, R. C., Ohno, H., Roche, K. W., and Bonifacino, J. S. (1997) Functional domain mapping of the clathrin-associated adaptor medium chains μ1 and μ2. *J. Biol. Chem.* **272,** 27160–27166
14. Hirst, J., Barlow, L. D., Francisco, G. C., Sahlender, D. A., Seaman, M. N., Dacks, J. B., and Robinson, M. S. (2011) The fifth adaptor protein complex. *PLoS Biol.* **9,** e1001170
15. Cosson, P., Démollière, C., Hennecke, S., Duden, R., and Letourneur, F. (1996) δ- and ζ-COP, two coatomer subunits homologous to clathrin-associated proteins, are involved in ER retrieval. *EMBO J.* **15,** 1792–1798
16. Martina, J. A., Bonangelino, C. J., Aguilar, R. C., and Bonifacino, J. S. (2001) Stonin 2: an adaptor-like protein that interacts with components of the endocytic machinery. *J. Cell Biol.* **153,** 1111–1120
17. Walther, K., Krauss, M., Diril, M. K., Lemke, S., Ricotta, D., Honing, S., Kaiser, S., and Haucke, V. (2001) Human stoned B interacts with AP-2 and synaptotagmin and facilitates clathrin-coated vesicle uncoating. *EMBO Rep.* **2,** 634–640
18. Reider, A., Barker, S. L., Mishra, S. K., Im, Y. J., Maldonado-Báez, L., Hurley, J. H., Traub, L. M., and Wendland, B. (2009) Syp1 is a conserved endocytic adaptor that contains domains involved in cargo selection and membrane tubulation. *EMBO J.* **28,** 3103–3116
19. Umasankar, P. K., Sanker, S., Thieman, J. R., Chakraborty, S., Wendland, B., Tsang, M., and Traub, L. M. (2012) Distinct and separable activities of the endocytic clathrin-coat components Fcho1/2 and AP-2 in developmental patterning. *Nat. Cell Biol.* **14,** 488–501
20. Owen, D. J., and Evans, P. R. (1998) A structural explanation for the recognition of tyrosine-based endocytotic signals. *Science* **282,** 1327–1332
21. Burgos, P. V., Mardones, G. A., Rojas, A. L., daSilva, L. L., Prabhu, Y., Hurley, J. H., and Bonifacino, J. S. (2010) Sorting of the Alzheimer's disease amyloid precursor protein mediated by the AP-4 complex. *Dev. Cell* **18,** 425–436
22. Jia, X., Singh, R., Homann, S., Yang, H., Guatelli, J., and Xiong, Y. (2012) Structural basis of evasion of cellular adaptive immunity by HIV-1 Nef. *Nat. Struct. Mol. Biol.* **19,** 701–706
23. Ohno, H., Fournier, M. C., Poy, G., and Bonifacino, J. S. (1996) Structural determinants of interaction of tyrosine-based sorting signals with the adaptor medium chains. *J. Biol. Chem.* **271,** 29009–29015
24. Dell'Angelica, E. C., Ohno, H., Ooi, C. E., Rabinovich, E., Roche, K. W., and Bonifacino, J. S. (1997) AP-3: an adaptor-like protein complex with ubiquitous expression. *EMBO J.* **16,** 917–928
25. Dell'Angelica, E. C., Klumperman, J., Stoorvogel, W., and Bonifacino, J. S. (1998) Association of the AP-3 adaptor complex with clathrin. *Science* **280,** 431–434
26. Peden, A. A., Oorschot, V., Hesser, B. A., Austin, C. D., Scheller, R. H., and Klumperman, J. (2004) Localization of the AP-3 adaptor complex defines a novel endosomal exit site for lysosomal membrane proteins. *J. Cell Biol.* **164,** 1065–1076
27. Sheffield, P., Garrard, S., and Derewenda, Z. (1999) Overcoming expression and purification problems of RhoGDI using a family of "parallel" expression vectors. *Protein Expr. Purif.* **15,** 34–39
28. Otwinowski, Z., and Minor, W. (1997) Processing of X-ray diffraction data collected in oscillation mode. *Methods in Enzymology* **276,** 307–326
29. Emsley, P., and Cowtan, K. (2004) Coot: model-building tools for molecular graphics. *Acta Crystallogr. D Biol. Crystallogr.* **60,** 2126–2132
30. Heldwein, E. E., Macia, E., Wang, J., Yin, H. L., Kirchhausen, T., and Harrison, S. C. (2004) Crystal structure of the clathrin adaptor protein 1 core. *Proc. Natl. Acad. Sci. U.S.A.* **101,** 14108–14113
31. Krissinel, E., and Henrick, K. (2007) Inference of macromolecular assemblies from crystalline state. *J. Mol. Biol.* **372,** 774–797
32. Collins, B. M., McCoy, A. J., Kent, H. M., Evans, P. R., and Owen, D. J. (2002) Molecular architecture and functional model of the endocytic AP2 complex. *Cell* **109,** 523–535
33. Kelly, B. T., McCoy, A. J., Späte, K., Miller, S. E., Evans, P. R., Höning, S., and Owen, D. J. (2008) A structural explanation for the binding of endocytic dileucine motifs by the AP2 complex. *Nature* **456,** 976–979
34. Jackson, L. P., Kelly, B. T., McCoy, A. J., Gaffry, T., James, L. C., Collins, B. M., Höning, S., Evans, P. R., and Owen, D. J. (2010) A large-scale conformational change couples membrane recruitment to cargo binding in the AP2 clathrin adaptor complex. *Cell* **141,** 1220–1229
35. Rohde, G., Wenzel, D., and Haucke, V. (2002) A phosphatidylinositol (4,5)-bisphosphate binding site within μ2-adaptin regulates clathrin-mediated endocytosis. *J. Cell Biol.* **158,** 209–214
36. Wang, Y. J., Wang, J., Sun, H. Q., Martinez, M., Sun, Y. X., Macia, E., Kirchhausen, T., Albanesi, J. P., Roth, M. G., and Yin, H. L. (2003) Phosphatidylinositol 4 phosphate regulates targeting of clathrin adaptor AP-1 complexes to the Golgi. *Cell* **114,** 299–310
37. Baust, T., Anitei, M., Czupalla, C., Parshyna, I., Bourel, L., Thiele, C., Krause, E., and Hoflack, B. (2008) Protein networks supporting AP-3 function in targeting lysosomal membrane proteins. *Mol. Biol. Cell* **19,** 1942–1951
38. Dell'Angelica, E. C., Shotelersuk, V., Aguilar, R. C., Gahl, W. A., and Bonifacino, J. S. (1999) Altered trafficking of lysosomal proteins in Hermansky-Pudlak syndrome due to mutations in the β 3A subunit of the AP-3 adaptor. *Mol. Cell* **3,** 11–21
39. Janvier, K., and Bonifacino, J. S. (2005) Role of the endocytic machinery in the sorting of lysosome-associated membrane proteins. *Mol. Biol. Cell* **16,** 4231–4242
40. Feng, L., Seymour, A. B., Jiang, S., To, A., Peden, A. A., Novak, E. K., Zhen, L., Rusiniak, M. E., Eicher, E. M., Robinson, M. S., Gorin, M. B., and Swank, R. T. (1999) The β3A subunit gene (Ap3b1) of the AP-3 adaptor complex is altered in the mouse hypopigmentation mutant pearl, a model for Hermansky-Pudlak syndrome and night blindness. *Hum. Mol. Genet.* **8,** 323–330
41. Kantheti, P., Qiao, X., Diaz, M. E., Peden, A. A., Meyer, G. E., Carskadon, S. L., Kapfhamer, D., Sufalko, D., Robinson, M. S., Noebels, J. L., and Burmeister, M. (1998) Mutation in AP-3 δ in the mocha mouse links endosomal transport to storage deficiency in platelets, melanosomes, and synaptic vesicles. *Neuron* **21,** 111–122
42. Mullins, C., Hartnell, L. M., Wassarman, D. A., and Bonifacino, J. S. (1999)

Defective expression of the μ3 subunit of the AP-3 adaptor complex in the *Drosophila* pigmentation mutant carmine. *Mol. Gen. Genet.* **262,** 401–412

43. Boll, W., Ohno, H., Songyang, Z., Rapoport, I., Cantley, L. C., Bonifacino, J. S., and Kirchhausen, T. (1996) Sequence requirements for the recognition of tyrosine-based endocytic signals by clathrin AP-2 complexes. *EMBO J.* **15,** 5789–5795
44. Rohrer, J., Schweizer, A., Russell, D., and Kornfeld, S. (1996) The targeting of Lamp1 to lysosomes is dependent on the spacing of its cytoplasmic tail tyrosine sorting motif relative to the membrane. *J. Cell Biol.* **132,** 565–576
45. Carvajal-Gonzalez, J. M., Gravotta, D., Mattera, R., Diaz, F., Perez Bay, A., Roman, A. C., Schreiner, R. P., Thuenauer, R., Bonifacino, J. S., and Rodriguez-Boulan, E. (2012) Basolateral sorting of the coxsackie and adenovirus receptor through interaction of a canonical YXXPhi motif with the clathrin adaptors AP-1A and AP-1B. *Proc. Natl. Acad. Sci. U.S.A.* **109,** 3820–3825
46. Gravotta, D., Carvajal-Gonzalez, J. M., Mattera, R., Deborde, S., Banfelder, J. R., Bonifacino, J. S., and Rodriguez-Boulan, E. (2012) The clathrin adaptor AP-1A mediates basolateral polarity. *Dev. Cell* **22,** 811–823
47. Ren, X., Farias, G. G., Canagarajah, B. J., Bonifacino, J. S., and Hurley, J. H. (2013) Structural basis for recruitment and activation of the AP-1 clathrin adaptor complex by Arf1. *Cell* **152,** 755–767
48. Wallace, A. C., Laskowski, R. A., and Thornton, J. M. (1995) LIGPLOT: a program to generate schematic diagrams of protein-ligand interactions. *Protein Eng.* **8,** 127–134